

ORIGINAL  
ARTICLECharacterization of a novel  
acetamidobenzoxazolone-based PET ligand for  
translocator protein (18 kDa) imaging of  
neuroinflammation in the brain

Anjani K. Tiwari,\*† Joji Yui,\* Masayuki Fujinaga,\* Katsushi Kumata,\*  
Yoko Shimoda,\* Tomoteru Yamasaki,\* Lin Xie,\* Akiko Hatori,\*  
Jun Maeda,\* Nobuki Nengaki\*‡ and Ming-Rong Zhang\*

\*Molecular Imaging Center, National Institute of Radiological Sciences, Chiba, Japan

†Division of Cyclotron and Radiopharmaceutical Sciences, Institute of Nuclear Medicine and Allied Sciences, Delhi, India

‡SHI Accelerator Service Co. Ltd., Tokyo, Japan

**Abstract**

We developed the novel positron emission tomography (PET) ligand 2-[5-(4-[<sup>11</sup>C]methoxyphenyl)-2-oxo-1,3-benzoxazol-3(2H)-yl]-N-methyl-N-phenylacetamide ([<sup>11</sup>C]MBMP) for translocator protein (18 kDa, TSPO) imaging and evaluated its efficacy in ischemic rat brains. [<sup>11</sup>C]MBMP was synthesized by reacting desmethyl precursor (**1**) with [<sup>11</sup>C]CH<sub>3</sub>I in radiochemical purity of ≥ 98% and specific activity of 85 ± 30 GBq/μmol (*n* = 18) at the end of synthesis. Biodistribution study on mice showed high accumulation of radioactivity in the TSPO-rich organs, e.g., the lungs, heart, kidneys, and adrenal glands. The metabolite analysis in mice brain homogenate showed 80.1 ± 2.7% intact [<sup>11</sup>C]MBMP at 60 min after injection. To determine the specific binding of [<sup>11</sup>C]MBMP with TSPO in the brain, *in vitro* autoradiography

and PET studies were performed in an ischemic rat model. *In vitro* autoradiography indicated significantly increased binding on the ipsilateral side compared with that on the contralateral side of ischemic rat brains. This result was supported firmly by the contrast of radioactivity between the ipsilateral and contralateral sides in PET images. Displacement experiments with unlabelled MBMP or PK11195 minimized the difference in uptake between the two sides. In summary, [<sup>11</sup>C]MBMP is a potential PET imaging agent for TSPO and, consequently, for the up-regulation of microglia during neuroinflammation.

**Keywords:** [<sup>11</sup>C]MBMP, microglia activation, neuroinflammation, positron emission tomography, translocator protein (18 kDa).

*J. Neurochem.* (2014) **129**, 712–720.

Microglia activation is the most predominant cellular response to inflammation within the central nervous system (CNS). This process is also characterized by a sharp change in the phenotype of these cells and by the over-expression of peripheral benzodiazepine receptor or, as recently proposed, translocator protein (18 kDa, TSPO) on the outer mitochondrial membranes of TSPO binding site (Papadopoulos *et al.* 2006a; Chauveau *et al.* 2008).

Over the past two decades, several researchers have demonstrated that the imaging of activated microglia in the CNS can be performed by positron emission tomography (PET) using TSPO ligands (Veneti *et al.* 2008; Batarseh and Papadopoulos 2010; Winkler *et al.* 2010; Trapani *et al.*

Received October 7, 2013; revised manuscript received January 11, 2014; accepted January 29, 2014.

Address correspondence and reprint requests to Ming-Rong Zhang, Molecular Probe Program, Molecular Imaging Center, National Institute of Radiological Sciences, 4-9-1 Anagawa, Inage-ku, Chiba 263-8555, Japan. E-mail: zhang@nirs.go.jp

**Abbreviations used:** % ID/g, percentage of the injected dose per gram of wet tissue; [<sup>11</sup>C]MBMP, 2-[5-(4-[<sup>11</sup>C]methoxyphenyl)-2-oxo-1,3-benzoxazol-3(2H)-yl]-N-methyl-N-phenylacetamide; BBB, blood–brain barrier; *BP<sub>ND</sub>*, binding potential; HPLC, high-performance liquid chromatography; MBMP, 2-[5-(4-methoxyphenyl)-2-oxo-1,3-benzoxazol-3(2H)-yl]-N-methyl-N-phenylacetamide; PET, positron emission tomography; SRTM, simplified reference-tissue model; SUV, standardized uptake value; TAC, time-activity curve; *t<sub>R</sub>*, retention time; TSPO, translocator protein (18 kDa).

2013). Radiolabelling of the isoquinoline-3-carboxamide derivative PK11195 with <sup>11</sup>C in the early 1980s paved way for the current concepts of PET imaging of neuroinflammation through TSPO ligands (Camsonne *et al.* 1984; Dolle *et al.* 2009). A number of PET ligands are being employed, such as benzodiazepine derivative [<sup>11</sup>C]Ro5-4864 (Watkins *et al.* 1988); phenoxyphenylacetamide derivatives [<sup>11</sup>C]DAA1106, [<sup>18</sup>F]FEDAA1106, and [<sup>11</sup>C]PBR28 (Zhang *et al.* 2003, 2004; Maeda *et al.* 2004; Hines *et al.* 2013); pyrimidineacetamide derivative [<sup>11</sup>C]DPA-713, [<sup>18</sup>F]DPA-714, and [<sup>11</sup>C]CLINME (Boutin *et al.* 2007; Van Camp *et al.* 2009, 2010; Arlicot *et al.* 2012); indoleacetamide derivative [<sup>11</sup>C]SSR180575 (Chauveau *et al.* 2011); and 8-oxopurine derivatives [<sup>11</sup>C]AC-5216 and [<sup>18</sup>F]FEDAC (Zhang *et al.* 2007; Yui *et al.* 2010). Although these PET ligands are promising and parts of them have been used to visualize TSPO in human brains, several issues need to be resolved before TSPO radioligands can be routinely used in clinical studies. It is necessary to find the optimal ligand showing requisite amounts of sensitivity and specificity and understand how TSPO polymorphisms can alter uptake of the PET ligands (Venneti *et al.* 2008; Owen *et al.* 2012; Kreisl *et al.* 2013; Venneti *et al.* 2013).

Following the development of [<sup>11</sup>C]DAA1106 (Zhang *et al.* 2003) and [<sup>11</sup>C]AC-5216 (Zhang *et al.* 2007), we are developing a new PET ligand for TSPO imaging. In this paper we have introduced a novel acetamidobenzoxazolone skeleton 2-[5-(4-methoxyphenyl)-2-oxo-1,3-benzoxazol-3(2H)-yl]-*N*-methyl-*N*-phenylacetamide (MBMP, Fig. 1) as a candidate ligand for TSPO. Recently, a group of researchers have prepared a library of acetamidobenzoxazolone derivatives as TSPO ligands (Fukaya *et al.* 2012). The selection of our candidate ligand, MBMP, was based on the pharmacophore model with high TSPO binding affinity ( $K_i = 0.29$  nM) and appropriate lipophilicity (computed  $\text{Log}D = 3.5$ ). The aim of our present study was to investigate the potential use of [<sup>11</sup>C]MBMP (Fig. 1) as a new PET ligand for neuroinflammation, and to demonstrate that this radioligand binds to TSPO sites, while having improved imaging properties over (*R*) [<sup>11</sup>C]PK11195.

## Materials and methods

### Chemicals and instrumentation

All chemicals were purchased from (Wako Pure Chemical Industries [Osaka, Japan], Tokyo Chemical Industries [Tokyo, Japan] and Sigma-Aldrich [Tokyo, Japan]), and used as received. Melting points were measured by a micro melting point apparatus (MP-500P). <sup>1</sup>H NMR (300 MHz) spectra were recorded on a JEOL-AL-300 NMR spectrometer (JEOL, Tokyo, Japan) with tetramethylsilane as an internal standard. Mass peaks were calculated by high-resolution fast atom bombardment (FAB) mass spectra, which were obtained and recorded on a JEOL JMS-Sx 102A spectrometer (JEOL). HPLC separation and analysis were performed using the JASCO HPLC system (JASCO, Tokyo, Japan).

Effluent radioactivity was monitored using a NaI (TI) scintillation detector system, and radioactivity measurement was performed during synthesis and animal studies with a Curiometer (Aloka, Tokyo, Japan).

### Chemical synthesis

#### 2-[5-(4-Methoxyphenyl)-2-oxo-1,3-benzoxazol-3(2H)-yl]-*N*-methyl-*N*-phenylacetamide (MBMP)

A mixture of 2-(5-bromo-2-oxo-1,3-benzoxazol-3(2H)-yl)-*N*-methyl-*N*-phenylacetamide (Fukaya *et al.* 2012) (1.44 g, 4.0 mmol) and 4-methoxyphenylboronic acid (729 mg, 4.8 mmol), K<sub>2</sub>CO<sub>3</sub> (829 mg, 6.0 mmol) and tetrakis(triphenylphosphine)palladium(0) (Pd(PPh<sub>3</sub>)<sub>4</sub>; 462 mg, 0.4 mmol) in 1,4-dioxane/water (3/1, 20 mL) was heated at 100°C under nitrogen atmosphere. The reaction mixture was stirred for 4 h and cooled to 25°C. Subsequently, the mixture was extracted with EtOAc. The organic layer was washed with brine and dried over sodium sulfate. After the solvent was removed *in vacuo*, and the residue was purified by silica gel column chromatography using hexane/EtOAc (2/1, v/v) as the eluent to give MBMP (1.23 g, 79.9% yield): white solid; mp 168–170°C (Fukaya *et al.* 2012). Chemical purity: > 99% by HPLC: Capcell Pack UG80 C<sub>18</sub> column (Shiseido, Tokyo, Japan), 4.6 mm i.d. × 250 mm; acetonitrile (MeCN)/H<sub>2</sub>O/Et<sub>3</sub>N, 6/4/0.01 (v/v/v); flow rate, 1.0 mL/min;  $\lambda_{\text{uv}}$ , 254 nm; retention time ( $t_R$ ), 10.1 min. <sup>1</sup>H NMR (CDCl<sub>3</sub>,  $\delta$ ) 3.32 (3H, s), 3.86 (3H, s), 4.35 (2H, s), 6.96–7.00 (3H, m), 7.19–7.23 (2H, m), 7.34 (2H, d,  $J = 7.7$  Hz), 7.41–7.54 (5H, m). high resolution mass spectrometer (HRMS) (FAB) calculated for C<sub>23</sub>H<sub>21</sub>O<sub>4</sub>N<sub>2</sub>, 389.1501; Observed:, 389.1511.

#### 2-[5-(4-Hydroxyphenyl)-2-oxo-1,3-benzoxazol-3(2H)-yl]-*N*-methyl-*N*-phenylacetamide (1)

Compound 1, as a desmethyl precursor for radiosynthesis, was prepared from 2-(5-bromo-2-oxo-1,3-benzoxazol-3(2H)-yl)-*N*-methyl-*N*-phenylacetamide (718 mg, 2.0 mmol) and 4-(4,4,5,5-tetramethyl-1,3,2-dioxaborolan-2-yl)phenol (528 mg, 2.4 mmol) in a manner similar to that described for MBMP, as a white solid (284 mg, 75.7% yield) after purification by silica gel column chromatography using hexane/EtOAc (1/1, v/v); mp: 202–205°C. Chemical purity: > 99% by HPLC: Capcell Pack UG80 C<sub>18</sub> column, 4.6 mm i.d. × 250 mm; MeCN/H<sub>2</sub>O/Et<sub>3</sub>N, 6/4/0.01 (v/v/v); flow rate, 1.0 mL/min;  $\lambda_{\text{uv}}$ , 254 nm;  $t_R$ , 3.0 min. <sup>1</sup>H NMR (DMSO-*d*<sub>6</sub>,  $\delta$ ): 3.22 (3H, s), 4.42 (2H, s), 6.86 (2H, d,  $J = 8.4$  Hz), 7.29–7.57 (10H, m), 9.56 (1H, s). HRMS (FAB) calculated for C<sub>22</sub>H<sub>19</sub>O<sub>4</sub>N<sub>2</sub>, 375.1345; observed, 375.1308.

#### 2-[5-(4-[<sup>11</sup>C]Methoxyphenyl)-2-oxo-1,3-benzoxazol-3(2H)-yl]-*N*-methyl-*N*-phenylacetamide ([<sup>11</sup>C]MBMP)

Cyclotron-produced [<sup>11</sup>C]CO<sub>2</sub> was bubbled into 0.4 M LiAlH<sub>4</sub> in anhydrous tetrahydrofuran (0.3 mL). After the evaporation of tetrahydrofuran, the remaining complex was treated with 57% hydroiodic acid (0.3 mL) to give [<sup>11</sup>C]CH<sub>3</sub>I, which was distilled with heating and transferred under N<sub>2</sub> gas flow to a solution of 1 (1 mg) and NaOH (5  $\mu$ L, 0.5 M) in *N,N*-dimethylformamide (DMF) (0.3 mL) at –15°C. After trapping was completed, this reaction mixture was heated at 70°C for 5 min. HPLC separation was performed on a Capcell Pack UG80 C<sub>18</sub> column (10 mm i.d. × 250 mm) using MeCN/H<sub>2</sub>O/Et<sub>3</sub>N (6/4/0.01, v/v/v) at 5.0 mL/min. The radioactive fraction corresponding to [<sup>11</sup>C]MBMP

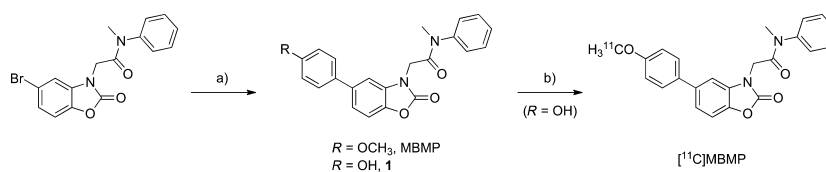


**Fig. 1** Chemical synthesis and radiosynthesis. Reagents and conditions: a)  $\text{Pd}(\text{PPh}_3)_4$ ,  $\text{K}_2\text{CO}_3$ , 4-substituted arylboron derivative,

1,4-dioxane/water (3/1), reflux, 4–5 h. b)  $[\text{11C}]\text{CH}_3\text{I}$ , NaOH, DMF,  $70^\circ\text{C}$ , 5 min.

( $t_R = 9.8$  min) was collected in a flask in which Tween 80 (0.075 mL) and ethanol (0.3 mL) was before the radiosynthesis. The fraction was evaporated to dryness, redissolved in 3 mL of sterile normal saline, and passed through a 0.22  $\mu\text{m}$  Millipore filter (Billerica, MA, USA). The identity of  $[\text{11C}]\text{MBMP}$  was confirmed by co-injection with unlabelled MBMP on a reverse phased–analytical HPLC on a Capcell Pack UG80  $\text{C}_{18}$  column (4.6 mm i.d.  $\times$  250 mm) using  $\text{MeCN}/\text{H}_2\text{O}/\text{Et}_3\text{N}$  (6/4/0.01, v/v/v) at 1.0 mL/min ( $t_R = 10.2$  min). In the final product solutions, their radiochemical purity was higher than 99% at the end of synthesis (EOS). No other significant peak was found on the HPLC chart. The specific activity was measured and calculated by comparing the assayed radioactivity with the mass measured at UV (254 nm). To determine the radiochemical stability of  $[\text{11C}]\text{MBMP}$ , after the formulated product solution was maintained for 30, 60, and 90 min at  $25^\circ\text{C}$ , analytic sample was taken from the solution to measure the radiochemical purity of  $[\text{11C}]\text{MBMP}$  with HPLC.

### $(R)[\text{11C}]\text{PK11195}$

The R enantiomer of  $[\text{11C}]\text{PK11195}$ , the standard PET ligand for TSPO, was synthesized as reported in the literature (Shah *et al.* 1994). The radiochemical purity of  $(R)[\text{11C}]\text{PK11195}$  was 99% and the specific activity was calculated as  $74 \pm 8$  GBq/ $\mu\text{mol}$  ( $n = 3$ ) at EOS.

### Animals

All animals were maintained and handled in accordance with the recommendations of the National Institute of Health and institutional guidelines of the National Institute of Radiological Sciences (NIRS). The experiments conducted in the NIRS were approved by the Animal Ethics Committee of the NIRS. Male ddY mice (male, 8 weeks old, 34–36 g) and Sprague–Dawley (SD) rats (male, 8–9 weeks old, 240–330 g) were purchased from Japan SLC (Shizuoka, Japan). The animals were housed under a 12/12-h dark/light cycle under optimal conditions. The ARRIVE guidelines were complied with.

### Biodistribution study

A saline solution of  $[\text{11C}]\text{MBMP}$  (5.6 MBq/0.08 nmol in 100  $\mu\text{L}$  per mouse) was injected into the ddY mice through the tail vein, and the mice were killed at five time intervals (1, 5, 15, 30, and 60 min). All ddY mice for each group ( $n = 4$ ) were killed by cervical dislocation after injection. Blood samples were acquired, and the cerebellum, cerebral cortex, other brain structures, liver, lungs, heart, kidneys, spleen, adrenal glands, small intestine, large intestine, and testes were quickly removed and weighed. The radioactivity in each tissue was measured using a gamma counter

(1480 Wizard 3, Perkin-Elmer, Waltham, MA, USA) and expressed as percentages of the injected dose per gram of wet tissue (% ID/g). All radioactivity measurements were corrected for decay.

### Radiolabelled metabolites analysis

The ddY mice were intravenously injected with  $[\text{11C}]\text{MBMP}$  (37–54 MBq/0.4–0.7 nmol,  $61 \pm 19$  GBq/ $\mu\text{mol}$  in 200–300  $\mu\text{L}$  per mouse) through the tail vein. The mice were killed by cervical dislocation at 5, 15, 30 or 60 min ( $n = 4$  for each point). Blood (0.7–1.0 mL) and whole brain samples were obtained and treated as reported previously (Zhang *et al.* 2003, 2004). The supernatant of plasma and brain homogenate was analyzed according to the following conditions: Capcell Pack UG80 $\text{C}_{18}$  column, 4.6 mm i.d.  $\times$  250 mm;  $\text{MeCN}/\text{H}_2\text{O}/\text{Et}_3\text{N}$ , 7/3/0.01 (v/v/v); flow rate, 1.0 mL/min. Percentages of the unchanged  $[\text{11C}]\text{MBMP}$  were calculated with correction of decay. At the same time, radioactivity fractions in the HPLC waste solution were measured using an auto-gamma counter.

### Ischemic model of rat brain

Mild focal ischemia was produced by intraluminal occlusion of the middle cerebral artery for 30 min using an intraluminal thread model (Yui *et al.* 2013). Briefly, a SD rat was anesthetized with 4% (v/v) isoflurane and maintained with 1.8% isoflurane. A ligation was conducted with the right internal carotid artery. A 4.0-monofilament nylon suture coated with silicon was inserted (16–18 mm) into the internal carotid artery up to the level of middle cerebral artery branches. The neck incision was closed with a silk suture. After regaining consciousness from anesthesia, the rats were reanesthetized after 30 min, and the filament was carefully removed for reperfusion. Throughout the surgery, the body temperature was monitored and maintained at an optimal level. All rats were employed for experiments 7 days after the surgery.

### In vitro autoradiography

Brain sagittal sections (10  $\mu\text{m}$ ) were prepared from frozen rat brains using a cryostat (HM560, Carl Zeiss, Oberkochen, Germany). The brain sections were pre-incubated for 20 min in 50 mM Tris-HCl buffer (pH 7.4) at  $25^\circ\text{C}$  followed by incubation in the same buffer containing  $[\text{11C}]\text{MBMP}$  (18 MBq, 0.2 nmol, 1 nM) at  $25^\circ\text{C}$  for 30 min. For the inhibition studies, unlabelled MBMP (10  $\mu\text{M}$ , prepared from 10 mM MBMP solution in distilled water containing 15% ethanol and 10% Tween 80) or PK11195 (10  $\mu\text{M}$ , prepared from 10 mM PK11195 solution in distilled water containing 15% ethanol and 10% Tween 80) was co-incubated with  $[\text{11C}]\text{MBMP}$ . After incubation, the brain sections were treated as reported previously (Yui *et al.* 2013). Autoradiograms were acquired using

a Bio-Imaging analyzer system (BAS-5000, Fujifilm, Tokyo, Japan). The radioactivity level on the brain regions was measured by the Multi Gauge analysis software version 2.3 (Fujifilm) and expressed as photo-stimulated luminescence per unit area (PSL/mm<sup>2</sup>).

### PET imaging

PET scans were conducted using a small-animal PET scanner (Inveon; Siemens Medical Solutions, Knoxville, TN, USA). Seven days after ischemic surgery, a rat was anesthetized with 1–2% isoflurane during the scan and its body temperature was maintained with a 40°C water circulation system (T/Pump TP401, Gaymar Industries, Orchard Park, NY, USA). An emission scan was immediately acquired for 60 min after injection of [<sup>11</sup>C]MBMP (37 MBq/0.4–0.6 nmol, 70 ± 21 GBq/μmol in 100 μL) or (*R*) [<sup>11</sup>C]PK11195 (37 MBq/0.5–0.7 nmol, 66 ± 10 GBq/μmol in 100 μL) through the tail vein. For the displacement experiments, respective unlabelled TSPO ligands (MBMP (1 mg/kg) or PK11195 (3 mg/kg) in 300 μL of saline containing 15% ethanol and 10% Tween 80) were injected 20 min after the injection of [<sup>11</sup>C]MBMP. Each experiment was performed in a group of three animals, and only one PET scan was performed with one animal.

### Image analysis

PET data modelling was performed into three-dimensional sinograms, which were changed into two-dimensional sinograms (frames × min: 4 × 1, 8 × 2, 8 × 5) by Fourier rebinning. Filtered back-projection using Hanning's filter with a Nyquist cut-off frequency of 0.5 cycle/pixel was used for dynamic image reconstruction. PET images were analyzed using ASIPro VM™ (Analysis Tools and System Setup/Diagnostics Tool; Siemens Medical Solutions) with reference to the magnetic resonance (MR) imaging template. A region of interest (ROI) with fixed size was manually positioned at the center of the striatum on the ipsilateral side defined on a summation image for each experiment, which coincided to the ROI used in autoradiography. The ipsilateral ROI was copied and symmetrically pasted into the contralateral striatum on the same slice to yield a contralateral ROI of identical volume and shape. Time-activity curves (TACs) for ipsilateral and contralateral striatum were generated. Decay correction was performed for the brain uptake of radioactivity with reference to the injection time and expressed as the standardized uptake value (SUV), which was normalized for the injected radioactivity and body weight. The SUV was calculated according to the following formula: SUV = (radioactivity per cubic centimetre tissue/injected radioactivity) × grams body weight.

The binding potential ( $BP_{ND}$ ) was calculated as a quantitative value, which represented the receptor binding with the radioligand, using PMOD software (PMOD Technologies, Zurich, Switzerland). The  $BP_{ND}$  was estimated using a simplified reference-tissue model (SRTM) by taking the TAC of the contralateral side as the reference region instead of the plasma input function. The SRTM analysis in the ipsilateral side of the striatum was performed using the TAC in the contralateral side as a reference region (Lammertsma and Hume 1996).  $R_1$  ( $k_1/k_1'$ ), which represented the ratio of tracer delivery, was estimated instead of input function.

### Statistical analysis

Statistical analyses were performed using SPSS software (IBM, Armonk, NY, USA) and Microsoft Office Excel 2007 (Microsoft,

Redmond, WA, USA). All data were expressed as the mean ± SD. For autoradiography, the changes in values were compared using Student's paired *t*-test. PET data were examined by one-way repeated-measure ANOVA. *p*-values less than 0.05 were considered statistically significant.

## Results

### Chemistry

Figure 1 shows the synthetic pathway for the synthesis of [<sup>11</sup>C]MBMP and its precursor **1** along with unlabelled MBMP. The desmethyl precursor **1** for radiosynthesis was synthesized by Suzuki's coupling reaction between the bromo compound and 4-(4,4,5,5-tetramethyl-1,3,2-dioxaborolan-2-yl)phenol in the presence of Pd(PPh<sub>3</sub>)<sub>4</sub>. For the synthesis of MBMP, 4-methoxyphenylboronic acid was used for coupling of the methoxyphenyl ring. The yield of both the reactions was 75.7% for **1** and 79.9% for MBMP. Proton NMR and high-resolution MS spectra confirmed the proposed stoichiometry and structure for the novel acetamidobenzoxazolone derivatives.

[<sup>11</sup>C]MBMP was synthesized by reacting precursor **1** with [<sup>11</sup>C]CH<sub>3</sub>I in the presence of NaOH in good radiochemical yields. After the reaction, separation, and formulation, 0.9–2.3 GBq (1.5 ± 0.6 GBq, *n* = 18) of [<sup>11</sup>C]MBMP was obtained after EOS, which started at 15.5–22.2 GBq (18.5 ± 2.1 GBq) of cyclotron-produced [<sup>11</sup>C]CO<sub>2</sub>. The specific activity was 50–130 GBq/μmol (85 ± 30 GBq/μmol, *n* = 18) at the end of the 32–36 min synthesis. The radiochemical purity of [<sup>11</sup>C]MBMP was higher than 99% and remained radiochemically stable for 1.5 h at 25°C. These analytical results were in compliance with our in-house quality control/assurance specifications.

### Biodistribution

Table 1 shows the biodistribution of radioactivity at the five time points after the injection of [<sup>11</sup>C]MBMP into the mice (*n* = 4 for each point). At 1 min, a high uptake of radioactivity (% ID/g) was shown immediately to reach a peak in the blood, heart, lung, and brain. In the lung, the radioactivity reached 160.8 ± 23.8% ID/g, which decreased very rapidly within 5 min to 60.3 ± 2.3% ID/g. The radioactivity in the adrenal glands increased until 60 min, whereas in other organs like the spleen and kidney it reached maximum on 15 min and then decreased. The initial brain uptake was higher than 2.0% ID/g at 1 min. The maximum amount of radioactivity was found in cerebellum. The uptake in the brain might be because of the lipophilic property of [<sup>11</sup>C]MBMP (cLogP = 3.5).

### Radiolabelled metabolites analysis

Up to 60 min after the injection of [<sup>11</sup>C]MBMP, only one radioactive metabolite peak was recovered from the plasma and brain tissues on radio-HPLC, in addition to intact [<sup>11</sup>C]

**Table 1** Radioactivity distribution in % ID/g of mice tissue ( $n = 4$ ) during 1–60 min time intervals

Organ/tissue	Time after the injection (min)					
	1	5	15	30	60	
Blood	1.98 ± 0.93	1.01 ± 0.12	0.49 ± 0.20	0.48 ± 0.02	0.47 ± 0.02	
Lung	160.80 ± 23.75	60.31 ± 2.29	34.17 ± 1.82	23.52 ± 2.76	16.96 ± 2.33	
Heart	17.21 ± 2.84	15.53 ± 0.91	13.80 ± 0.66	8.19 ± 1.36	5.91 ± 0.54	
Liver	0.99 ± 0.15	2.92 ± 0.27	3.09 ± 0.34	3.05 ± 0.56	2.81 ± 0.48	
Spleen	3.12 ± 0.96	9.05 ± 0.39	12.06 ± 2.34	10.30 ± 1.13	9.82 ± 0.76	
Adrenal gland	4.95 ± 2.11	12.95 ± 3.05	16.88 ± 4.55	18.26 ± 6.77	21.78 ± 7.27	
Kidney	8.27 ± 0.50	13.55 ± 0.87	15.66 ± 1.88	14.94 ± 1.13	13.51 ± 0.95	
S. Intestine	1.41 ± 0.31	2.76 ± 0.22	2.62 ± 0.21	2.53 ± 0.34	2.73 ± 0.29	
L. Intestine	0.79 ± 0.15	1.51 ± 0.22	1.75 ± 0.20	1.64 ± 0.26	1.65 ± 0.07	
Testis	0.41 ± 0.20	0.72 ± 0.03	0.82 ± 0.07	0.97 ± 0.09	1.23 ± 0.13	
Cerebral cortex	2.43 ± 0.40	1.84 ± 0.18	1.12 ± 0.28	0.58 ± 0.07	0.53 ± 0.09	
Cerebellum	2.53 ± 0.58	2.41 ± 0.18	1.48 ± 0.43	1.15 ± 0.08	0.80 ± 0.17	
Other brain structures	2.26 ± 0.21	1.92 ± 0.12	1.16 ± 0.25	0.72 ± 0.08	0.53 ± 0.03	

**Table 2** Metabolite analysis of [ $^{11}\text{C}$ ]MBMP in the plasma and brain of mice ( $n = 4$  at each time point)

Time after the injection (min)	Percentage (%) in the plasma	Percentage (%) in the brain
5	64.9 ± 4.6	98.6 ± 0.5
15	38.0 ± 5.3	94.3 ± 0.5
30	24.1 ± 2.2	83.4 ± 1.8
60	21.0 ± 1.9	65.7 ± 2.7

MBMP ( $t_R = 6.6$  min). Table 2 shows the percentages of intact [ $^{11}\text{C}$ ]MBMP in the plasma and brain. The fraction corresponding to intact [ $^{11}\text{C}$ ]MBMP in the plasma gradually decreased to  $21.0 \pm 1.9\%$  at 60 min after the injection. However, in the brain, intact [ $^{11}\text{C}$ ]MBMP ( $98.6 \pm 0.5\%$ ) was detected with one polar metabolite ( $t_R = 2.9$  min) at 5 min. After 60 min the intactness of [ $^{11}\text{C}$ ]MBMP in the brain was  $65.7 \pm 2.7\%$ . The recovery of radioactivity from HPLC analysis for all samples was greater than 95%.

### *In vitro* autoradiography

Figure 2 shows the *in vitro* autoradiographic results of [ $^{11}\text{C}$ ]MBMP on the ischemic rat brain. In the control section (a), the ipsilateral side (right) showed high radioactive signal levels compared with the contralateral side (left). However, the difference in radioactivity levels between the contralateral and ipsilateral sides was diminished by co-incubation with an excess of unlabelled MBMP (b) or PK11195 (c). In the control sections, the ratio of radioactive signals in the ipsilateral side compared with the contralateral side was approximately 4 : 1. In the brain sections treated with unlabelled MBMP or PK11195, the ratio of radioactive signals in the ipsilateral side compared with the contralateral side was approximately 1. Compared with the control, the

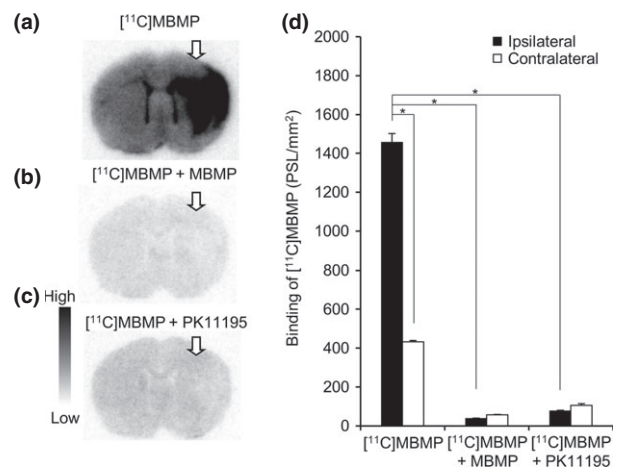


**Fig. 2** *In vitro* autoradiographic results of 2-[5-(4-[ $^{11}\text{C}$ ]methoxyphenyl)-2-oxo-1,3-benzoxazol-3(2*H*)-yl]-*N*-methyl-*N*-phenylacetamide ([ $^{11}\text{C}$ ]MBMP) in ischemic rat brains ( $n = 4$ ). Arrows indicate ischemic areas. Representative autoradiograms of [ $^{11}\text{C}$ ]MBMP alone (a) or with unlabelled MBMP (b) or with PK11195 (c) were depicted in identical scales. Quantitative effects of unlabelled MBMP or PK11195 on the *in vitro* binding of [ $^{11}\text{C}$ ]MBMP on brain sections (d). Radioactivity concentrations determined in the brain regions are expressed as photo-stimulated luminescence (PSL)/mm<sup>2</sup>. \* $p < 0.05$ .

treatment with unlabelled MBMP or PK11195 indicated a large reduction of ipsilateral binding (Fig. 2,  $-97.4\%$  for unlabelled MBMP and  $-94.7\%$  for PK11195).

### PET

Figure 3 shows representative PET/MR images and TACs in the brain of ischemic rats treated with [ $^{11}\text{C}$ ]MBMP (a, b) and (*R*)[ $^{11}\text{C}$ ]PK11195 (c, d), respectively. The PET study showed that [ $^{11}\text{C}$ ]MBMP and (*R*)[ $^{11}\text{C}$ ]PK11195 had higher uptakes in the ipsilateral side than in the contralateral side. Initially, the maximum uptake was  $1.35 \pm 0.12$  SUV for [ $^{11}\text{C}$ ]MBMP

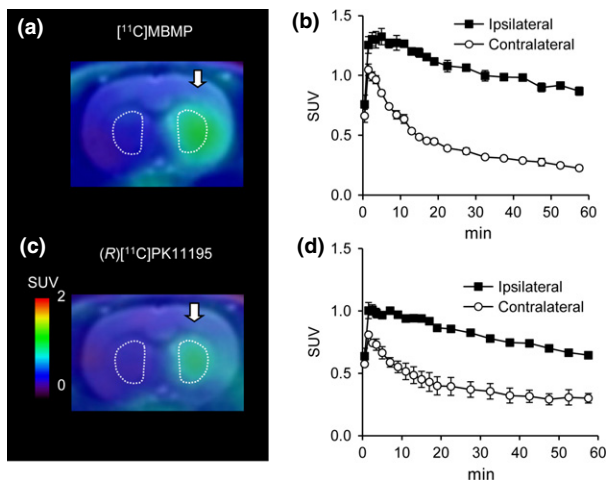


**Fig. 3** Coronal positron emission tomography (PET) images and time-activity curves for 2-[5-(4-[<sup>11</sup>C]methoxyphenyl)-2-oxo-1,3-benzoxazol-3(2*H*)-yl]-*N*-methyl-*N*-phenylacetamide ([<sup>11</sup>C]MBMP) (a, b) and (*R*) [<sup>11</sup>C]PK11195 (c, d) in ischemic rat brains ( $n = 3$ ). PET images (a, c) were generated by summation of whole scans (0–60 min) and were overlaid on magnetic resonance images as anatomical templates of normal rat brain. Arrows indicate ischemic areas. Curves (b, d) were plotted based on the PET images of the ipsilateral and contralateral striatum. Significant difference ( $p < 0.05$ ) was observed between two sides.

(B) and  $1.00 \text{ SUV} \pm 0.42$  ( $p < 0.05$ ) for (*R*) [<sup>11</sup>C]PK11195 (d). In the contralateral side at 60 min after injection, lower uptake of [<sup>11</sup>C]MBMP ( $0.23 \pm 0.03 \text{ SUV}$ ) was observed in comparison with that of (*R*) [<sup>11</sup>C]PK11195 ( $0.33 \pm 0.05 \text{ SUV}$ ,  $p < 0.1$ ). A high ipsilateral to contralateral ratio was observed for [<sup>11</sup>C]MBMP, which was significantly higher than (*R*) [<sup>11</sup>C]PK11195 ( $2.77 \pm 0.42$  vs.  $1.80 \pm 0.18$ ,  $p < 0.01$ ).

In addition, the PET quantitative value of the ligand bound to the receptor was presented as the  $BP_{ND}$ , which were non-invasively obtained by SRTM analysis using the contralateral side as the reference region. The  $BP_{ND}$  values in the ipsilateral sides were  $2.03 \pm 0.24$  for [<sup>11</sup>C]MBMP and  $1.24 \pm 0.39$  ( $p < 0.05$ ) for (*R*) [<sup>11</sup>C]PK11195. The  $R_1$  values instead of the input function were  $1.14 \pm 0.05$  for [<sup>11</sup>C]MBMP and  $1.12 \pm 0.08$  ( $p = 0.82$ ) for (*R*) [<sup>11</sup>C]PK11195.

The displacement studies are shown in Fig. 4. The treatment with unlabelled MBMP or PK11195 at 20 min after injection of [<sup>11</sup>C]MBMP minimized the heterogeneous radioactive signals between the ipsilateral and contralateral sides in PET images, respectively (b, e). When unlabelled MBMP or PK11195 was injected 20 min after the injection of [<sup>11</sup>C]MBMP, as shown in their TACs (c, f), the uptake of radioactivity in the ipsilateral side was lowered to a level similar to that in the contralateral side. From 30 min to the end of the PET scan, there was no difference in the radioactivity uptake between the ipsilateral and contralateral

sides. These data indicate that displacement with unlabelled MBMP or PK11195 significantly reduced [<sup>11</sup>C]MBMP binding in the ipsilateral side.

## Discussion

In this study, we have synthesized [<sup>11</sup>C]MBMP, which is the first PET ligand derivatized from a novel skeleton, acetamidobenzoxazolone, for TSPO imaging. The *in vivo* studies demonstrated that [<sup>11</sup>C]MBMP crosses the blood–brain barrier (BBB) with observable brain uptake within a few min and interacts selectively with TSPO without significant interference from radiolabelled metabolites.

Neuroinflammation changes microglial morphology and results in the over-expression of TSPO. The number of cases of neuroinflammation and neurodegenerative disorders has multiplied many fold in the last two decades, which requires more non-invasive monitoring techniques and novel diagnostic markers (Dolle *et al.* 2009). TSPO is expressed at low levels on astrocytes and resting microglial cells in a healthy brain (Gulyás *et al.* 2011). However, its levels are markedly increased during neuroinflammation and, subsequently, in neurodegeneration. Moreover, TSPO may be important in modulating neuronal damage and, hence, may support accelerated microglial proliferation (Papadopoulos *et al.* 2006b). Therefore, PET imaging of TSPO can provide excellent information as a diagnostic tool in the early stages of neurodegenerative disorders (Casellas *et al.* 2002; Chen and Guilarte 2008; Takano *et al.* 2010; Lavisse *et al.* 2012). The reference radioligand (*R*) [<sup>11</sup>C]PK11195 has not gained wide acceptance as a PET imaging agent because of persistent problems with its quantification *in vivo*. To date, nearly 75–80 TSPO radioligands, which can be classified into 7–8 chemical classes, have been developed (Watkins *et al.* 1988; Maeda *et al.* 2004; Zhang *et al.* 2004, 2007; Van Camp *et al.* 2009, 2010).

Several new radioligands have been assessed in human subjects, including [<sup>11</sup>C]DAA1106, [<sup>18</sup>F]FEDAA1106, [<sup>11</sup>C]PBR28, [<sup>11</sup>C]vinpocetine, [<sup>11</sup>C]AC-5216, [<sup>11</sup>C]DPA713, and [<sup>18</sup>F]DPA714 (Van Camp *et al.* 2009; Yui *et al.* 2010; Arlicot *et al.* 2012). However, the human studies of these clinically used TSPO PET ligands are at their preliminary stages with relatively small databases. Of these, [<sup>11</sup>C]DAA1106 and [<sup>11</sup>C]PBR28 have shown binding capability in diseased human living brain in Alzheimer and schizophrenic conditions (Venneti *et al.*, 2009; Takano *et al.* 2010; Kreisl *et al.* 2013).

Our candidate molecule, MBMP, shows a similar binding affinity for TSPO ( $K_i$ : 0.29 nM) (Fukaya *et al.* 2012) to other well-established TSPO ligands of second generation. To develop the optimal ligand for human clinical application to be accepted widely, we synthesized [<sup>11</sup>C]MBMP to demonstrate that [<sup>11</sup>C]MBMP binds to TSPO sites *in vitro* and *in*

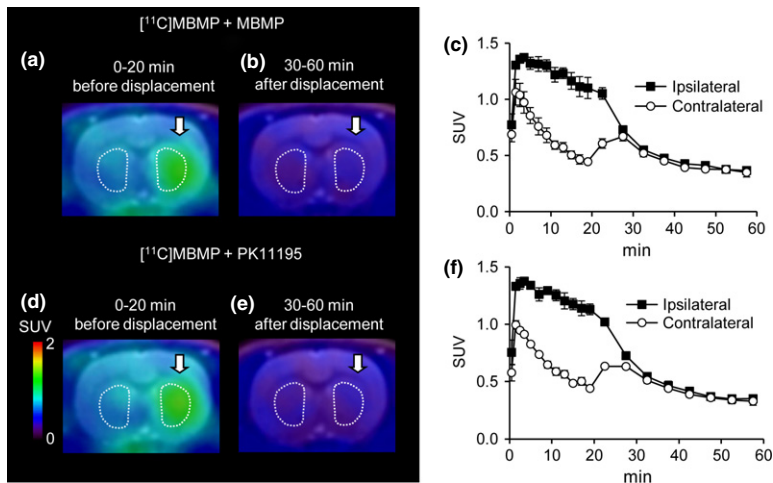


**Fig. 4** Coronal positron emission tomography (PET) images and time-activity curves for 2-[5-(4- $^{11}\text{C}$ )methoxyphenyl]-2-oxo-1,3-benzoxazol-3(2*H*)-yl]-*N*-methyl-*N*-phenylacetamide ( $^{11}\text{C}$ ]MBMP) with unlabelled MBMP (1 mg/kg;  $n = 3$ ) or PK11195 (3 mg/kg;  $n = 3$ ) were determined in ischemic rat brains. Arrows indicate ischemic areas. PET images were generated by summation of the early phase (0–20 min) before treatment with unlabelled MBMP (a) or PK11195 (d) and the late phase (30–60 min) after treatment with unlabelled MBMP (b) or PK11195 (e). Curves (c, f) were plotted based on the PET images of the ipsilateral and contralateral striatum.

*in vivo*, while having improved imaging properties over (*R*) $^{11}\text{C}$ ]PK11195.

The biodistribution of radioligand is an important characteristic to study because it demonstrates how the radioligand will distribute *in vivo* and how it excretes. The present biodistribution study revealed that the majority of the radioactivity was distributed in prominent TSPO-expressing organs (Table 1). Low radioactivity uptake was found in low TSPO expressing major organs, such as the liver ( $\leq 3.0\%$  ID/g). The radioactivity distribution in mouse brains showed fast penetration across the BBB into all brain regions at 1 min after injection, which was highest in the cerebellum, the region with relatively high TSPO expression in normal rodent brain (Zhang *et al.* 2003; Maeda *et al.* 2004).

After the injection of  $^{11}\text{C}$ ]MBMP, only one radiolabelled metabolite was detected by radio-HPLC in the plasma and brain homogenates of the mice. As indicated by its  $t_R$  of 2.9 min, the metabolite was more polar than  $^{11}\text{C}$ ]MBMP ( $t_R = 6.6$  min). The metabolite in the brain showed the same  $t_R$  as the metabolite found in the plasma. This result confirmed the slow metabolism of  $^{11}\text{C}$ ]MBMP in the brain or, in general, a limited level ( $< 35\%$  at 60 min after injection) of radiolabelled metabolite originating from the plasma routed to the brain. Therefore, this result certified that the brain uptake was mainly because of  $^{11}\text{C}$ ]MBMP itself.

Because of the low TSPO expression in normal brain, we used an ischemic rat model in which TSPO expression is elevated by neuroinflammation with microglial activation. Our previous study had indicated that the ischemic surgery did not cause widespread disruption and serious breakdown of BBB (Yui *et al.* 2010). In fact,  $R_1$ , the tracer delivery ratio between the ipsilateral and contralateral sides, was close to unity both for  $^{11}\text{C}$ ]MBMP and (*R*) $^{11}\text{C}$ ]PK11195. This result suggests that the brain uptake of  $^{11}\text{C}$ ]MBMP and (*R*) $^{11}\text{C}$ ]PK11195 determined in this study was mostly because of specific uptake and minimally affected by a potential disruption of BBB.

The *in vitro* autoradiography indicated that  $^{11}\text{C}$ ]MBMP bound with TSPO-rich lesions and enhanced radioligand binding by more than 3.9-fold in the ipsilateral area compared with the contralateral side (Fig. 2). The contrast between the ipsilateral and contralateral sides disappeared in the presence of an excess of MBMP or PK 11195, which demonstrated the specificity of the *in vitro* binding with TSPO.

The PET study with  $^{11}\text{C}$ ]MBMP confirmed that uptake was significantly higher in the ipsilateral side than in the contralateral side, which allowed clear visualization of the lesion site on the PET images (Fig. 3).  $^{11}\text{C}$ ]MBMP was completely displaced from the ipsilateral area by an excess of the corresponding MBMP or PK11195 and, within minutes, reached the level of uptake in the contralateral area (Fig. 4). Moreover,  $^{11}\text{C}$ ]MBMP showed a higher ratio of ipsilateral to contralateral uptakes and higher  $BP_{ND}$  than (*R*) $^{11}\text{C}$ ]PK11195 under the same experimental conditions, suggesting higher *in vivo* specific binding of  $^{11}\text{C}$ ]MBMP for TSPO in the brain.

In the present study, although  $^{11}\text{C}$ ]MBMP showed higher  $BP_{ND}$  than  $^{11}\text{C}$ ]PK11195 in the same ischemic model, this new tracer may not have significant advantage over second generation TSPO radioligands.  $^{11}\text{C}$ ]MBMP has the similar *in vitro* binding affinity for TSPO with those TSPO radioligands. More importantly, approximately 35% radiolabelled metabolite of  $^{11}\text{C}$ ]MBMP was found in the mouse brain at 60 min after the ligand injection, whereas only less than 10% radiolabelled metabolite of those TSPO radioligands was in the rodent brains (Zhang *et al.* 2003, 2004; Boutin *et al.* 2007; Van Camp *et al.* 2009, 2010; Arlicot *et al.* 2012). This property is likely to hamper the clinical application of  $^{11}\text{C}$ ]MBMP. Therefore, we will not perform further evaluation for  $^{11}\text{C}$ ]MBMP, including comparison with the TSPO radioligands of second generation and determination of the selectivity of  $^{11}\text{C}$ ]MBMP for low and high affinity TSPO binding sites described with those ligands (Owen *et al.* 2011).

In conclusion, [<sup>11</sup>C]MBMP was easily labelled by using <sup>11</sup>C with high radiolabelling efficiency and showed favorable biodistribution pattern, and high *in vitro* and *in vivo* specific binding for TSPO. Optimization for [<sup>11</sup>C]MBMP is in progress.

## Acknowledgments and conflict of interest disclosure

The authors would like to thank the staff at the National Institute of Radiological Sciences for their support with the cyclotron operation, radioisotope production, radiosynthesis, and animal experiments. This study was supported by under NIRS-IAEA program 2013. The first author is also grateful to Dr R. P. Tripathi, Director, Institute of Nuclear Medicine and Allied Sciences (INMAS), Delhi for their support and assistance. All experiments were conducted in compliance with the ARRIVE guidelines. The authors have no conflict of interest to declare.

## References

- Arlicot N., Vercouillie J., Ribeiro M. J. *et al.* (2012) Initial evaluation in healthy humans of [<sup>18</sup>F]DPA-714, a potential PET biomarker for neuroinflammation. *Nucl. Med. Biol.* **39**, 570–578.
- Batarsch A. and Papadopoulos V. (2010) Regulation of translocator protein 18 kDa (TSPO) expression in health and disease states. *Mol. Cell. Endocrinol.* **327**, 1–12.
- Boutin H., Chauveau F., Thominiaux C., Grégoire M. C., James M. L., Trebossen R., Hantraye P., Dollé F., Tavitian B. and Kassiou M. (2007) <sup>11</sup>C-DPA-713: a novel peripheral benzodiazepine receptor PET ligand for *in vivo* imaging of neuroinflammation. *J. Nucl. Med.* **48**, 573–581.
- Camsonne R., Crouzel C., Comar D., Maziere M., Prenant C., Sastre J., Moulin M. A. and Syrota A. (1984) Synthesis of N-[<sup>11</sup>C]-methyl, N-(methyl-1-propyl), (chloro-2-phenyl)-1-isoquinoline carboxamide-3 (PK11195): a new ligand for peripheral benzodiazepine receptors. *J. Labelled Comp. Radiopharm.* **21**, 985–991.
- Casellas P., Galiegue S. and Basile A. S. (2002) Peripheral benzodiazepine receptors and mitochondrial function. *Neurochem. Int.* **40**, 475–486.
- Chauveau F., Boutin H., Van Camp N., Dollé F. and Tavitian B. (2008) Nuclear imaging of neuroinflammation: a comprehensive review of [<sup>11</sup>C]PK 11195 challengers. *Eur. J. Nucl. Med. Mol. Imaging* **35**, 2304–2319.
- Chauveau F., Boutin H., Van Camp N. *et al.* (2011) *In vivo* imaging of neuroinflammation in the rodent brain with [<sup>11</sup>C]SSR180575, a novel indoleacetamide radioligand of the translocator protein (18 kDa). *Eur. J. Nucl. Med. Mol. Imaging* **38**, 509–514.
- Chen M. K. and Guilarte T. R. (2008) Translocator protein 18 kDa (TSPO): molecular sensor of brain injury and repair. *Pharmacol. Ther.* **118**, 1–17.
- Dolle F., Luus C., Reynolds A. and Kassiou M. (2009) Radiolabelled molecules for imaging the translocator protein (18 kDa) using positron emission tomography. *Curr. Med. Chem.* **16**, 2899–2923.
- Fukaya T., Kodo T., Ishiyama T., Kakuyama H., Nishikawa H., Baba S. and Masumoto S. (2012) Design, synthesis and structure–activity relationships of novel benzoxazolone derivatives as 18 kDa translocator protein (TSPO) ligands. *Bioorg. Med. Chem.* **20**, 5568–5582.
- Gulyás B., Vas Á., Tóth M. and Takano A. (2011) Age and disease related changes in the translocator protein (TSPO) system in the human brain: positron emission tomography measurements with [<sup>11</sup>C]vinpocetine. *Neuroimage* **56**, 1111–1121.
- Hines C. S., Fujita M., Zoghbi S. S. *et al.* (2013) Propofol decreases *in vivo* binding of <sup>11</sup>C-PBR28 to translocator protein (18 kDa) in the human brain. *J. Nucl. Med.* **54**, 64–69.
- Kreisl W. C., Lyoo C. H., McGwier M. *et al.* (2013) *In vivo* radioligand binding to translocator protein correlates with severity of Alzheimer's disease. *Brain* **136**, 2228–2238.
- Lammertsma A. A. and Hume S. P. (1996) Simplified reference tissue model for PET receptor studies. *Neuroimage* **4**, 153–158.
- Lavisse S., Guillermier M., Hérard A. S. *et al.* (2012) Reactive astrocytes overexpress TSPO and are detected by TSPO positron emission tomography imaging. *J. Neurosci.* **32**, 10809–10818.
- Maeda J., Suhara T., Zhang M. R. *et al.* (2004) Peripheral benzodiazepine receptor ligand [<sup>11</sup>C]DAA1106 for PET: an imaging tool for glial cells in the brain. *Synapse* **52**, 283–291.
- Owen D. R., Gunn R. N., Rabiner E. A. *et al.* (2011) Mixed affinity binding in humans with 18-kDa translocator protein ligands. *J. Nucl. Med.* **52**, 24–32.
- Owen D. R., Yeo A. J., Gunn R. N. *et al.* (2012) An 18-kDa translocator protein (TSPO) polymorphism explains differences in binding affinity of the PET radioligand PBR28. *J. Cereb. Blood Flow Metab.* **32**, 1–5.
- Papadopoulos V., Baraldi M., Guilarte T. R. *et al.* (2006a) Translocator protein (18 kDa): New nomenclature for the peripheral-type benzodiazepine receptor based on its structure and molecular function. *Trends Pharmacol. Sci.* **27**, 402–409.
- Papadopoulos V., Lecanu L., Brown R. C., Han Z. and Yao Z. X. (2006b) Peripheral-type benzodiazepine receptor in neurosteroid biosynthesis, neuropathology and neurological disorders. *Neuroscience* **138**, 749–756.
- Shah F., Hume S. P., Pike V. W., Ashworth S. and McDermott J. (1994) Synthesis of the enantiomers of [N-methyl-<sup>11</sup>C]PK 11195 and comparison of their behaviours as radioligands for PK binding sites in rats. *Nucl. Med. Biol.* **21**, 573–581.
- Takano A., Arakawa R., Ito H., Tateno A., Takahashi H., Matsumoto R., Okubo Y. and Suhara T. (2010) Peripheral benzodiazepine receptors in patients with chronic schizophrenia: a PET study with [<sup>11</sup>C]DAA1106. *Int. J. Neuropsychopharmacol.* **13**, 943–950.
- Trapani A., Palazzo C., de Candia M., Lasorsa F. M. and Trapani G. (2013) Targeting of the translocator protein 18 kDa (TSPO): a valuable approach for nuclear and optical imaging of activated microglia. *Bioconjug. Chem.* **24**, 1415–1428.
- Van Camp N., Boisgard R., Kuhnast B. *et al.* (2009) Comparative evaluation of the translocator protein radioligands <sup>11</sup>C-DPA-713, <sup>18</sup>F-DPA-714, and <sup>11</sup>C-PK 11195 in a rat model of acute neuroinflammation. *J. Nucl. Med.* **50**, 468–476.
- Van Camp N., Boisgard R., Kuhnast B. *et al.* (2010) *In vivo* imaging of neuroinflammation: a comparative study between [(18F)]PBR111, [(11C)]CLINME and [(11C)]PK11195 in an acute rodent model. *Eur. J. Nucl. Med. Mol. Imaging* **37**, 962–972.
- Venneti S., Wang G. J., Nguyen J. and Wiley C. A. (2008) The positron emission tomography ligand DAA1106 binds with high affinity to activated microglia in human neurological disorders. *J. Neuropathol. Exp. Neurol.* **67**, 1001–1010.
- Venneti S., Lopresti B. J. and Wiley C. A. (2013) Molecular imaging microglial/macrophage in the brain. *Glia* **61**, 10–23.
- Watkins G. L., Jewett D. M., Mulholland G. K., Kilbourn M. R. and Toorongian S. A. (1988) A captive solvent method for rapid N-[<sup>11</sup>C]methylation of secondary amides: application to the Benzodiazepine, 4'-chlorodiazepam (RO5-4864). *Int. J. Rad. Appl. Instrum. A* **39**, 441–444.
- Winkeler A., Boisgard R., Martin A. and Tavitian B. (2010) Radioisotopic imaging of neuroinflammation. *J. Nucl. Med.* **51**, 1–4.

- Yui J., Maeda J., Kumata K., Kawamura K., Yanamoto K., Hatori A., Yamasaki T., Nengaki N., Higuchi M. and Zhang M. R. (2010)  $^{18}\text{F}$ -FEAC and  $^{18}\text{F}$ -FEDAC: PET of the monkey brain and imaging of translocator protein (18 kDa) in the infarcted rat brain. *J. Nucl. Med.* **51**, 1301–1309.
- Yui J., Xie L., Fujinaga M., Yamasaki T., Hatori A., Kumata K., Nengaki N. and Zhang M. R. (2013) Monitoring neuroprotective effects using positron emission tomography with [ $^{11}\text{C}$ ]TMM, a radiotracer for metabotropic glutamate 1 receptor. *Stroke* **44**, 2567–2572.
- Zhang M. R., Kida T., Noguchi J., Furutsuka K., Maeda J., Suhara T. and Suzuki K. (2003) [ $^{11}\text{C}$ ]DAA1106: radiosynthesis and *in vivo* binding to peripheral benzodiazepine receptors in mouse brain. *Nucl. Med. Biol.* **30**, 513–519.
- Zhang M. R., Maeda J., Ogawa M., Noguchi J., Ito T., Yoshida Y., Okauchi T., Obayashi S., Suhara T. and Suzuki K. (2004) Development of a new radioligand, *N*-(5-fluoro-2-phenoxyphenyl)-*N*-(2-[ $^{18}\text{F}$ ]fluoroethyl-5-methoxybenzyl)acetamide, for PET imaging of peripheral benzodiazepine receptor in primate brain. *J. Med. Chem.* **47**, 2228–2235.
- Zhang M. R., Kumata K., Maeda J., Yanamoto K., Hatori A., Okada M., Higuchi M., Obayashi S., Suhara T. and Suzuki K. (2007)  $^{11}\text{C}$ -AC-5216: a novel positron emission tomography ligand for peripheral-type benzodiazepine receptors in primate brain. *J. Nucl. Med.* **48**, 1853–1861.